12th International Conference on Fracture Mechanics of Concrete and Concrete Structures
FraMCoS-12
B.L.A. Pichler, Ch. Hellmich, P. Preinstorfer (Eds)

https://doi.org/10.21012/FC12.1243
MS18-3:1

PERFORMANCE OF NOVEL 3D APPROACH WITH EXPLICIT DEFINITION OF FIBRES-CONCRETE INTERACTION IN PREDICTING THE FRC/FRHPC RESPONSE

IRENEUSZ MARZEC[*] AND JERZY BOBIŃSKI[*]

[*] Gdańsk University of Technology, Faculty of Civil and Environmental Engineering
11/12 Gabriela Narutowicza Street, 80-233 Gdańsk, Poland
e-mail: ireneusz.marzec@pg.edu.pl, jerzy.bobinski@pg.edu.pl

Key words: Fibre reinforced concrete (FRC), Finite Element Method (FEM), crack propagation, fracture

Abstract: The motivation for this study is a new material design for wave energy convertor floater hull, which requires exceptional performance in harsh marine environment under extreme weather conditions. Fibre reinforced concrete (FRC) utilises its highest performance after initial cracking, exhibiting strain-hardening when the cracks bridged by fibres redistribute the stresses over larger volume of concrete and thus increase the load bearing capacity of the specimen. The proper numerical description of cracks is of major importance to obtain physically meaningful results for high performance concrete (HPC) reinforced with alternative reinforcements like short fibres or textile reinforcement. Thus, the goal is to introduce the numerical tool in order to investigate the behaviour of FRC and FRHPC members. Since, such tool can be calibrated for a given type of fibres, then for any new concrete mixes, if only the properties of plain concrete are known, one can easily estimates the influence of steel fibres additive without necessity to proceed additional series of experiments. The main idea of presented approach is to assume the fully 3D modelling with taking into account explicitly the distribution and orientation of the steel-fibres embedded in 3D concrete continuum. Moreover, an explicit bond-slip interaction between each fibre and concrete is implemented. Consequently, different failure modes associated with fibres pull-out or fibres rupture can be independently simulated. As a benchmark, results obtained from experimental campaign on different specimens made from concrete with steel fibres of different sizes and dosages were taken. Results of numerical simulations were directly compared with experimental outcomes in order to validate and calibrate FE-model and to introduce the efficient numerical modelling tool.

1 INTRODUCTION

The accurate numerical description of cracks is crucial for obtaining physically meaningful results in concrete or high-performance concrete (HPC), especially when reinforced with alternative materials like short fibres or textile reinforcements. The bond behaviour, reinforcement stiffness, and nonstandard properties of fibre-reinforced concrete (FRC) or high-performance concrete (FRHPC) result in a distinct strain and crack distribution compared to traditional steel-reinforced concrete members. In general, cracks in concrete can be described using smeared approaches [1] within elastoplasticity or damage mechanics, displacement discontinuities with cohesive elements [2], or advanced methods like the eXtended Finite Element Method, Discrete Element Method [3, 4], or beam lattice models [5].

This study focuses on the numerical simulations of low-carbon HPC with steel fibres for the hulls of wave energy converters (WECs). These structures must endure harsh marine conditions and extreme pressures for a service life of at least 25 years. WEC hulls face significant hydrostatic pressure, especially during critical load scenarios when submerged several meters underwater. A hollow structure weighing hundreds tons, with a diameter of about 20 meters and a height of 4 meters, must be robust enough to resist such forces. A honeycomb internal structure to support the external walls was developed, which are primarily subjected to compressive forces. Despite the theoretically pure compression state of the internal walls under critical loads, other factors - such as thermal gradients during casting, shrinkage, and wave slamming - induce combined compression and flexural stresses, potentially causing cracks. FRC performs exceptionally well after initial cracking, as fibres bridge the cracks, redistribute stresses, and enhance the load-bearing capacity. The post-cracking behaviour of FRC depends on fibre type, geometry, content, stiffness, and the quality of the bond between the fibres and the concrete matrix. Fibre orientation is also a crucial factor, especially in thin-walled elements, where geometry often aligns fibres in specific directions, making FRC anisotropic.

Understanding the composite behaviour of FRC/FRHPC, particularly in relation to fibre content and bond performance, is supported by numerical modelling. Two primary modelling approaches exist. The first treats FRC as a homogeneous material, incorporating fibres indirectly through an equivalent constitutive law. This "continuous type" approach simplifies the analysis by considering only one constitutive relationship, often using RILEM recommendations for material definition in tension, which assume linear elasticity up to the peak, followed by trilinear softening. This method is effective for simulating large-scale specimens. For example, Abbas et al. [6] modelled the performance of steel fibre-reinforced concrete beam-column joints under seismic loading, while Liu et al. [7] used a similar approach to study tunnel linings, comparing numerical simulations with full-scale tests.

The second approach explicitly represents fibres within the concrete matrix, allowing for detailed analysis of their distribution and interactions. Mellios et al. [8] used computed tomography (CT) scans to capture real fibre topology and applied elastic-perfectly plastic models for steel fibres. Zhao et al. [9] coupled computational fluid dynamics (CFD) with finite element method (FEM) to simulate the casting process of self-compacting steel fibre-reinforced concrete. Other studies, like those by Xu et al. [10] and Gal and Kryvoruk [11], used mesoscale models to account for aggregates, cement matrix, interfacial transition zones, and fibre-matrix bonds, providing highly detailed simulations.

Explicit models also address fibre-matrix slip, a key factor in FRC performance. Some of them assume perfect bonding, while other ones incorporate slip through connector elements, modified constitutive laws, or advanced techniques like interface elements. Recent innovations include Zhang et al.'s [12] "shadow elements" and Huang et al.'s "fibre channel elements" [13], both implemented in Abaqus for detailed 2D simulations. These techniques enable nuanced analyses of fibre-concrete interactions, offering valuable insights for designing FRC structures capable of withstanding extreme environmental conditions.

The paper aims to present a numerical tool for analysing the behaviour of FRC and FRHPC members. Using FEA and a direct 3D mesoscale modelling approach, the tool replaces costly and time-consuming experiments by simulating the impact of specific fibre types on various concrete mixes. Once calibrated for a given fibre type, the model allows for quick predictions of steel fibre effects in new concrete formulations, provided the properties of plain concrete are known, eliminating the need for extensive experimental testing. Unlike the 2D approaches in [12] and [13], this model operates within a fully 3D framework.

2 METHOD

The primary concept of the presented approach is to employ full 3D modelling while explicitly accounting for the distribution and orientation of steel fibres embedded within a 3D concrete continuum. The material behaviour is described using the following constitutive laws: coupled damaged plasticity with isotropic softening for concrete, and a simple 1D elastic-plastic criterion with isotropic hardening/softening for steel. To explicitly include the fibres' presence, individually modelled fibres are incorporated into the 3D framework. The fibres topology is randomly generated based on a predefined three-directional intensity field, enabling the introduction of directional bias in fibres orientations. This enhanced directionally-dependent generator facilitates the modelling of fibres-reinforced concrete (FRC) anisotropy, reflecting variations in fibres alignment due to factors such as casting direction or specimen geometry.

To model the interaction between fibres and concrete, interface (connector) elements are introduced between the concrete matrix and fibres allowing for detailed interaction modelling.

2.1 Model for concrete

The concrete was described as a homogeneous material using a non-local coupled elasto-plastic-damage formulation [14]. A detailed discussion of this formulation, including its advantages and limitations, is provided in [14]. The authors' approach for modeling concrete under monotonic and cyclic loading integrates elasto-plasticity with scalar isotropic damage, based on the strain equivalence hypothesis [15]. This constitutive model has been successfully applied in the analysis of various reinforced concrete (RC) members subjected to diverse loading conditions and failure modes. Elasto-plasticity is defined within the effective stress space. For elasto-plastic behavior, the Rankine and Drucker-Prager criteria with linear hardening are adopted, where the hardening modulus is set to $E/2$ (E being the Young's modulus). Material softening is characterized using isotropic damage, with the equivalent strain measure $\tilde{\varepsilon}$ definition based on total strains, following the approach proposed by Mazars [16]:

$$\tilde{\varepsilon} = \sqrt{\sum \langle \varepsilon_i \rangle^2} \tag{1}$$

where ε_i is a principal strain. The state variable κ and two additional quantities κ_t and κ_c to describe stiffness degradation in tension and softening, respectively, are defined as:

$$\kappa = \max_{\tau \le t} \tilde{\varepsilon}(\tau), \kappa_t = r\kappa, \ \kappa_c = (1-r)\kappa, \tag{2}$$

where r is a triaxiality factor [17]:

$$r(\boldsymbol{\sigma}) = \begin{cases} 0 & \text{if} \quad \sigma_i = 0 \\ \dfrac{\sum \langle \sigma_i \rangle}{\sum |\sigma_i|} & \text{otherwise.} \end{cases} \tag{3}$$

Symbol $\langle \sigma_i \rangle$ stands for a positive value of a principal stress σ_i and symbol $|\sigma_i|$ denotes an absolute value of a principal stress σ_i. The degradation parameter D is described via the formula:

$$D = 1 - (1 - s_c D_t)(1 - s_c D_c), \tag{4}$$

where s_c and s_t are splitting functions:

$$s_t = 1 - a_t r(\boldsymbol{\sigma}) \text{ and } s_c = 1 - a_c\big(1 - r(\boldsymbol{\sigma})\big) \tag{5}$$

The degradation parameter in tension D_t is defined with following formula:

$$D_t = 1 - \frac{\kappa_0}{\kappa_t}\big(1 - \alpha + \alpha \exp\big(-\beta(\kappa_t - \kappa_0)\big)\big), \tag{6}$$

with the state variable κ_t and parameters κ_0, α, and β. The degradation parameter in compression is calculated using the relationship (after [18]):

$$\begin{aligned} D_c = 1 - \left(1 - \frac{\kappa_0}{\kappa_c}\right)\left(0.01 - \frac{\kappa_0}{\kappa_c}\right)^{\eta_1} + \\ - \left(\frac{\kappa_0}{\kappa_c}\right)^{\eta_2} \exp\big(-\delta_c(\kappa_c - \kappa_0)\big). \end{aligned} \tag{7}$$

The parameters η_1, η_2 and δ_c are utilized in the model. It is important to note that the same value of κ_0 is used to calculate both degradation parameters D_t and D_c. A comprehensive description and further details regarding the performance of the model are provided in [14].

To accurately reproduce strain localization, restore the well-posedness of the boundary

value problem, and account for deterministic size effect, an integral-type non-local theory is employed as a regularisation technique in this coupled model. This approach has been proved to preserve compliance with thermodynamic principles. As a result, the local value of the variable controlling the material softening is replaced with its non-local counterpart, calculated as an averaged quantity over neighbouring points, using the following formula:

$$\bar{\varepsilon}(\boldsymbol{x}) = \frac{\int_V w(\|\boldsymbol{x}-\boldsymbol{\xi}\|)\tilde{\varepsilon}(\boldsymbol{\xi})\mathrm{d}\boldsymbol{\xi}}{\int_V w(\|\boldsymbol{x}-\boldsymbol{\xi}\|)\mathrm{d}\boldsymbol{\xi}}. \tag{8}$$

Here, $\boldsymbol{x}$ represents the considered point, and $\boldsymbol{\xi}$ denotes the neighboring points. The weighting function w is defined using a Gaussian distribution (l_c – characteristic length):

$$w(r) = \frac{1}{l_c\sqrt{\pi}}\exp\left(-\left(\frac{r}{l_c}\right)^2\right). \tag{9}$$

2.2 Steel fibres

To describe the behaviour of steel fibres, a simple 1D elastic-plastic constitutive law was assumed, characterized by the modulus of elasticity E_s, yield stress σ_y and linear softening. Each fibre was explicitly modelled as an individual rod using 2-node linear truss elements (T3D2 according to Abaqus nomenclature). To capture the real characteristics of steel fibres, two distinct regions were defined for each fibre (Fig. 1). For the regions in ends (10 mm length) of the fibre the modified cross section A_1 maybe assumed (note it can be reduced, but not necessarily) in order to better capture the influence of anchorage zone characteristic. In turn, the region in middle of fibre (40 mm length) was with cross section A_2 corresponding to the actual cross-section of the Dramix5D fibre. All fibres were explicitly distributed and oriented within the concrete domain (Fig. 2). The fibres were placed explicitly within the 3D concrete volume without any alignment or coincidence with the finite element (FE) mesh of the concrete domain. In other words, the FE mesh for the steel elements was independent of the FE mesh for the concrete elements. Rather than aligning the nodes of one mesh to the other to establish interactions between the two domains, the embedded region technique was employed. This approach, implemented using the embedded element method in Abaqus, enables a group of elements to be embedded within "host" elements. The Abaqus solver automatically determines geometric relationships between the nodes of the embedded (steel fibres) elements and the host (concrete) elements. If a node of a steel fibre lies within a concrete element, the node's translational degrees of freedom are eliminated, and it becomes an "embedded node". These degrees of freedom are then constrained to the interpolated values of the corresponding degrees of freedom of the host element [19]. Consequently, the translational degrees of freedom for the nodes of steel fibres were constrained to match those of the surrounding concrete elements, based on the given topology of the independent meshes and a specified tolerance.

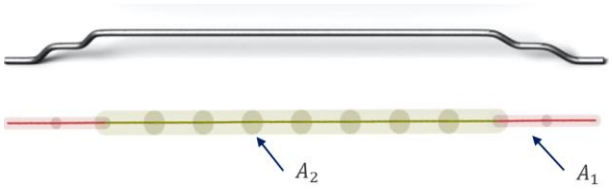

Figure 1: Dramix 5D steel fibre and its numerical representation.

2.3 Fibres – concrete interaction

A bond-slip law between each fibre and the surrounding concrete was implemented, maintaining the same topology of the meshes - without any direct coincidence between them. The approach involves the use of user-defined elements as connectors to enforce the bond-slip law. To achieve this, "additional" nodes were introduced and positioned at the same coordinates as the "steel" nodes (Fig. 3). These "additional" nodes were constrained to the "concrete" nodes using a technique similar to the simplified embedded element method provided by Abaqus. Interaction between the "steel" nodes and the constrained "additional"

nodes was then modelled through interface elements. Specifically, 4-node user-defined elements with zero thickness were created based on the pairs of "steel" and "additional" nodes (Fig. 3). It is worth noting that the distance between "steel" and "additional" nodes shown in Fig. 3 is artificial and presented only for clarity.

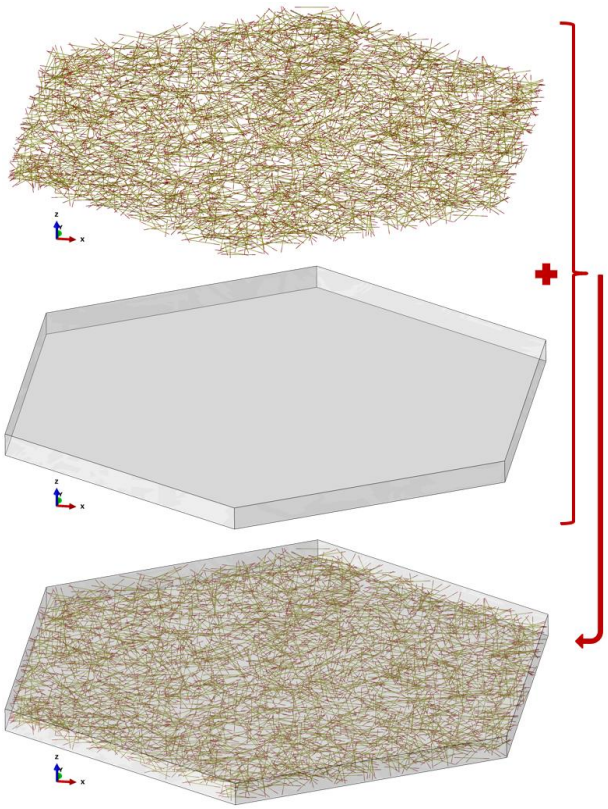

Figure 2: Idea of 3D-modeling, taking into account steel fibres with actual geometry explicitly and randomly embedded in concrete domain.

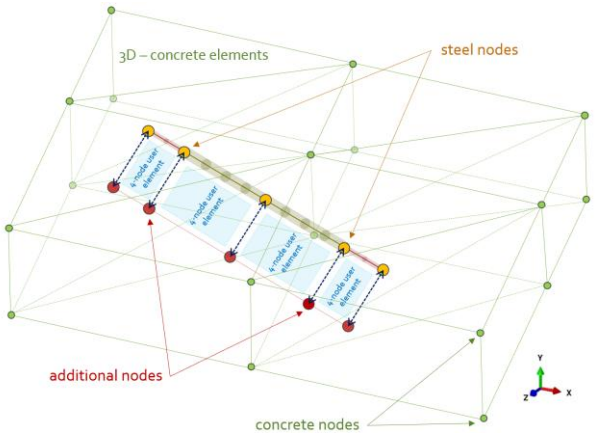

Figure 3: A schematic representation of the presented approach utilising user interface elements constructed from "steel" and "additional" nodes.

The use of user-defined interface elements enables the implementation of arbitrary bond-slip interactions along the contact line. The fundamental equations and detailed description underlying the above presented method are detailed in [20].

The preliminary implemented bond-slip relationships follow well-established functions from the literature, originally proposed for standard reinforcing bars. As an initial study, the bond-slip relationship between shear traction and slip was modelled according to the formulation by Dörr [21], and its performance was thoroughly investigated. This bond law neglects softening and assumes a yield plateau once the displacement reaches a defined limit:

$$\tau_b = \begin{cases} f_t \left(0.5\left(\frac{\delta}{\delta_0}\right) - 4.5\left(\frac{\delta}{\delta_0}\right)^2 + 1.4\left(\frac{\delta}{\delta_0}\right)^3 \right) & \text{if } 0 < \delta < \delta_0 \\ 1.9 f_t & \text{if } \delta > \delta_0 \end{cases} \tag{10}$$

where, δ_0 represents the displacement at which perfect slip occurs, and f_t denotes the tensile strength of concrete. Alternatively, the bond-slip law based on the CEB-FIB code [22] was employed. In this case, the relationship between the bond shear stress and slip is expressed as follows:

$$\tau_b = \begin{cases} \tau_{\max} \left(\frac{\delta}{\delta_1}\right)^{\alpha} & 0 < \delta \le \delta_1 \\ \tau_{\max} & \delta_1 < \delta \le \delta_2 \\ \tau_{\max} - (\tau_{\max} - \tau_f)\frac{\delta - \delta_1}{\delta_3 - \delta_2} & \delta_2 < \delta \le \delta_3 \\ \tau_f & \delta_3 < \delta \end{cases} \tag{11}$$

In this formulation, α is a parameter with a default value of 0.2. Since the functions described above were originally developed for ribbed bars, key constants such as f_t, $\tau_{\max}$, δ_0, δ_1, etc. must be appropriately adjusted for fibres. Defining these parameter values for fibre-reinforced concrete (FRC) or fibre-reinforced high-performance concrete (FRHPC) is inherently challenging. While some fundamental parameters can be directly obtained from experimental data, others require calculation using assumed or derived analytical formulas. Alternatively, they may be determined through inverse analysis of experimental results.

Defining the input data for the analysed problem involves several sequential steps. First,

the concrete domain must be established by specifying the geometry, boundary conditions, loads, material definitions, and section assignments. Following this, the definitions of fibres, including nodes and elements, should either be imported or manually defined. Once the fibre definitions are prepared, they are embedded into the concrete domain using the embedded element technique available in Abaqus. After embedding, a text input file is generated from the Abaqus model. The next step involves duplicating the fibre node definitions, retaining their original coordinates while assigning new node labels to the duplicates. The fibre elements are then redefined by replacing the original node labels with those of their duplicates. Additionally, zero-material elements, defined as truss or beam elements with identical topology to the original fibre elements but zero material (no output stiffness and no output stresses), must be created. Finally, 4-node user interface elements are defined based on the topology of the original fibres, with each element incorporating two original nodes and their corresponding duplicate nodes. The initial steps, including defining the geometry, materials, and loads, as well as generating the input file, can be entirely executed within the Abaqus/CAE environment. This provides flexibility without imposing restrictions on the geometry or other modelling parameters. However, reproducing the fibres topology effectively requires the use of a directionally dependent generator. This external generator produces a fibres topology adapted to the specific boundary shape of the structural member, incorporating anisotropy through directional bias in fibres orientations. The generated fibres geometry is then imported into Abaqus as a separate part. To execute the subsequent steps, involving modifications to node and element definitions, additional scripts are highly beneficial, although a spreadsheet application with text file import/export functionality can also be employed. Abaqus does not natively support interface elements with linear geometry in 3D (3D equivalence of COH2D4 elements). As such, custom code must be developed to define these elements, using quaternions to transform their orientation from the global coordinate system to local one. Furthermore, the material law, including regularisation techniques, and the bond-slip law must also be implemented. While it is possible to utilise built-in material definitions within Abaqus for user elements, certain limitations apply. The final output of the entire process is a modified input file containing all necessary information for analysis. It should be emphasized that the proposed framework primarily addresses topological considerations and imposes no restrictions on the constitutive modelling of concrete, steel, or the slip-bond relationship. Alternative constitutive models can be implemented as needed (the only limit here is the availability of the source code).

3 RESULTS

As a benchmark test results from experimental tests for planar elements in the form of thin, hexagonal panels tested under bending were utilised. The motivation for using such samples resulted from their representation of a critical section in the wave energy floater's structure. Under real ocean conditions, this section is primarily subjected to uniform hydrostatic pressure. For simplification, the distributed load was replaced with a concentrated load applied at the centre of the panel. The panels were subjected to monotonic loading until failure, with continuous monitoring of deflections and crack development. The bending test of these members was conducted using a custom-designed support structure made of steel elements to ensure uniform stiffness at all support points (located at the mid-span of each edge, as shown in Fig. 4). The load was distributed to the supports via 40×40 mm rubber bricks to promote uniform deformation. The panels were centrally loaded under displacement control using an Instron 5980 testing machine.

The finite element (FE) results of preliminary calculations for FRHPC panels under bending are presented in Figures 5, 6, 7 and 8. Figure 5 compares the numerically calculated force-displacement (F-u) curves with experimental data for simulations

employing the bond-slip law defined according to Dörr's formulation. A satisfactory agreement was achieved between the calculated and experimental results, with both showing very similar pre- and post-cracking behaviour. Decreasing the displacement parameter δ_0 and increasing the concrete tensile strength f_t resulted in a stiffer panel response.

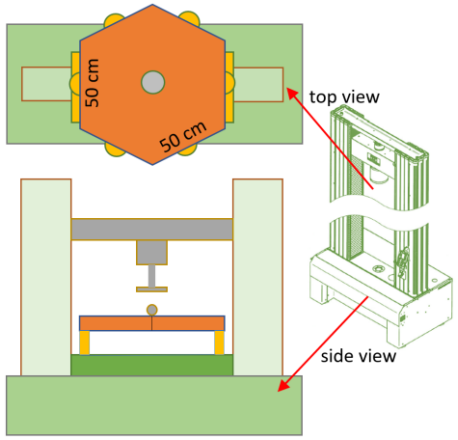

Figure 4: A schematic representation of experimental testing setup for hexagonal panels.

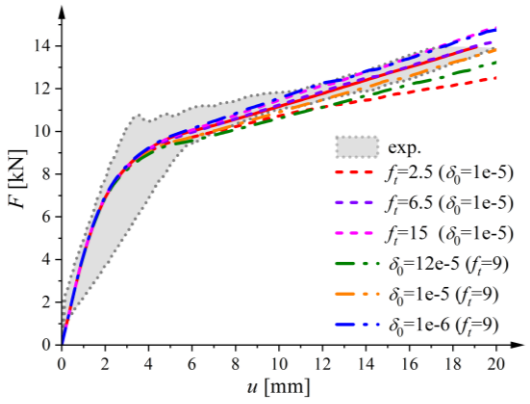

Figure 5: Calculated force – deflection curves as compared to experiments for FRC panels under bending for different parameters of bond-law according to Dörr's formulation.

Similarly, FE results for simulations using the bond-slip law defined by the CEB-FIB formulation are shown in Figure 6. Comparable trends were observed, with a stiffer response achieved by decreasing the displacement parameter δ_1 and increasing the ultimate shear strength τ_{max} (Fig. 6). The results for both Dörr and CEB-FIB formulations, are closely aligned.

Figure 7 illustrates the calculated distributions of the non-local equivalent strain measure in concrete alongside the experimental crack patterns. The overall failure behaviour, characterized by multiple centrally spreading cracks, was accurately reflected. In regions where concrete cracking occurred, a significant increase in the von Mises equivalent stress in the steel fibres was observed (indicated by red areas in Figure 8). Furthermore, the stress levels in the fibres were influenced by their orientation - fibres oriented perpendicularly to the cracks exhibited notably higher stress levels, as shown by the red areas in Figure 8.

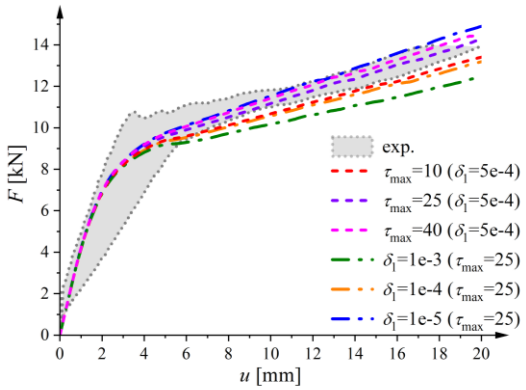

Figure 6: Calculated force – deflection curves as compared to experiments for FRC panels under bending for different parameters of bond-law according to CEB-FIB formulation.

4 SUMMARY

From the preliminary FE simulations of FRHPC members, several basic conclusions can be drawn. The simulations demonstrated satisfactory agreement with experimental results in terms of both force-displacement curves and strain localization patterns. The presented approach offers significant potential for controlling the overall material response and proved capable of simulating the realistic characteristics of the composite, particularly the influence of the number of fibres.

Nevertheless, some issues remain that require further consideration. Thus, further investigations of the performance of above-presented approach is needed. The attention will be focused on influence of different parameters in context of proper calibration of

the slip-bond law and enhancements of directionally dependent generator for fibres in order to predicting the FRC/FRHPC characteristics for different types and volume amount of fibres.

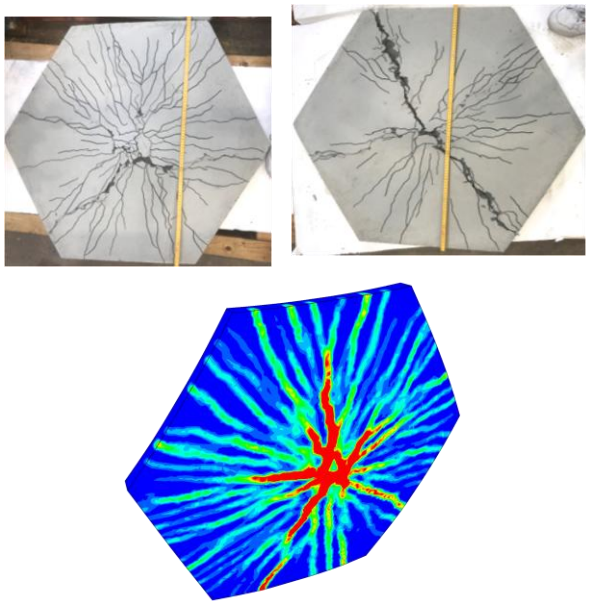

Figure 7: Calculated distributions of non-local equivalent strain measure in concrete as compared to experimental crack pattern for FRC.

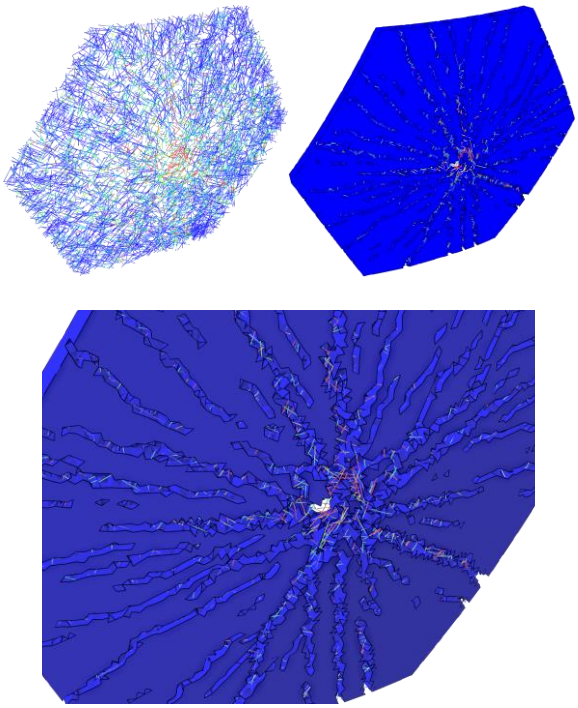

Figure 8: Calculated distributions of von Mises equivalent stress in steel fibres for FRC panels under bending (degraded concrete elements are excluded from the view).

ACKNOWLEDGEMENTS

Computations were carried out using the computers of Centre of Informatics Tricity Academic Supercomputer & Network. This research was partially funded by National Centre for Research and Development and Clean Energy Transition Partnership (CETP) co-funded by the European Union within project WECHULL+ "Sustainable Concrete Material Leading to Improved Substructures for Offshore Renewable Energy Technologies" (CETP-2022-00127).

REFERENCES

[1] Grassl, P., Xenos, D., Nystrom, U., Rempling, R., Gylltoft, K., 2013. CDPM2: a damage-plasticity approach to modelling the failure of concrete. International *Journal of Solids and Structures*. **50**: 3805–3816.

[2] Zhou, F., Molinari, J.F., 2004. Dynamic crack propagation with cohesive elements: a methodology to address mesh dependency. *International Journal for Numerical Methods in Engineering*. **59**(1):1–24

[3] Moes, N., Belytschko, T., 2002. Extended finite element method for cohesive crack growth. *Engineering Fracture Mechanics.* **69**(7): 813–833.

[4] Nitka, M., Tejchman, J., 2015. Modelling of concrete behaviour in uniaxial compression and tension with DEM. *Granular Matter*. **17**:145-164.

[5] Sun, B., Huang, X., Zheng, Y., Guo, L., 2020. Multi-scale lattice method for mesoscopic crack growth simulation of concrete structures. *Theoretical and Applied Fracture Mechanics*. **106**: 102475.

[6] Abbas, A., Mohsin, S., Cotsovos, M., 2014. Seismic response of steel fiber reinforced concrete beam-column joints. *Engineering Structures*. **59**:261-283.

[7] Liu, X., Sun, Q., Song, W., Bao, Y., 2022. Numerical modelling and parametric study of hybrid fiber-rebar reinforced concrete tunnel linings. *Engineering Structures*. **251**:113565.

[8] Mellios, N., Oesch, T., Spyridis, P., 2022.

Finite element modelling of UHPC under pulsating load using X-ray computed tomography based fiber distributions. *Materials and Structures*. **55**(1).

[9] Zhao, Y. , Bi, J., Huo, L., Wang, Z., Guan, J., 2021. Development of a coupled numerical framework of steel fiber reinforced self-compacting concrete. *Construction and Building Materials*. **303**:124582.

[10] Xu, Z., Hao, H., Li, H.N., 2012. Mesoscale modelling of dynamic tensile behaviour of fibre reinforced concrete with spiral fibres. *Cement and Concrete Research*. **42**(11):1475–1493.

[11] Gal, E., Kryvoruk, R., 2011. Meso-scale analysis of FRC using a two-step homogenization approach. *Computers and Structures*. **89**:921-929.

[12] Zhang, H., Huang, Y., Xu, S., Natarajan, S., Yao, F., 2023. An explicit methodology of random fibre modelling for FRC fracture using non-conforming meshes and cohesive interface elements. *Composite Structures*. **310**: 116762.

[13] Huang, Y., Huanf, J., Zhang, W., Liu, X., 2023. Experimental and numerical study of hooked-end steel fiber-reinforced concrete based on the meso- and macro-models. *Composite Structures*. **309**: 116750.

[14] Marzec, I., Tejchman, J., 2022. Experimental and numerical investigations on RC beams with stirrups scaled along height or length. *Engineering Structures* **252**:113621.

[15] Pamin, J., de Borst, R., 1999. Stiffness degradation in gradient-dependent coupled damage-plasticity. *Archives of Mechanics.* **51(**3-4):419-446.

[16] Mazars, J., 1986. A description of micro- and macroscale damage of concrete structures. *Engineering Fracture Mechanics.* **25** (5-6): 729–737.

[17] Lee, J., Fenves, G.L., 1998. Plastic-damage model for cyclic loading of concrete structures. *Journal of Engineering Mechanics ASCE* **124**(8): 892–900.

[18] Geers, M.G.D., 1997. *Experimental Analysis and Computational Modeling of Damage and Fracture*. PhD Thesis, Eindhoven University of Technology.

[19] Abaqus Documentation. *Dassault Systemes*. 2016.

[20] Marzec, I., Suchorzewski, J., Bobiński, J. 2024. Three dimensional simulations of FRC beams and panels with explicit definition of fibres-concrete interaction. *Engineering Structures* **319**:118856.

[21] Dörr, K., 1980. *Ein Beitag zur Berechnung von Stahlbetonscheiben unter Berücksichtigung des Verbundverhaltens*. PhD Thesis. Darmstadt University.

[22] *CEB-FIP model code 1990*. 1993. CEB-FIB.